

Prograde rotation of protoplanets by accretion of pebbles in a gaseous environment

Anders Johansen^{1*} and Pedro Lacerda^{2,3}

¹*Leiden Observatory, Leiden University, P.O. Box 9513, 2300 RA Leiden, The Netherlands*

²*Queen's University, Belfast, County Antrim, BT7 1NN, United Kingdom*

³*Newton Fellow*

Accepted 200- January -. Received 200- January -; in original form 200- January -

ABSTRACT

We perform hydrodynamical simulations of the accretion of pebbles and rocks onto protoplanets of a few hundred kilometres in radius, including two-way drag force coupling between particles and the protoplanetary disc gas. Particle streams interacting with the gas far out within the Hill sphere of the protoplanet spiral into a prograde circumplanetary disc. Material is accreted onto the protoplanet due to stirring by the turbulent surroundings. We speculate that the trend for prograde rotation among the largest asteroids is primordial and that protoplanets accreted 10%–50% of their mass from pebbles and rocks during the gaseous solar nebula phase. Our model also offers a possible explanation for the narrow range of spin periods observed among the largest bodies in the asteroid and trans-Neptunian belts, and predicts that 1000 km-scale Kuiper belt objects that have not experienced giant impacts should preferentially spin in the prograde direction.

Key words: hydrodynamics – Kuiper belt – minor planets, asteroids – planetary systems: protoplanetary disks – planets: rings – Solar system: formation

1 INTRODUCTION

Planets form in protoplanetary gas discs as dust grains collide and grow to ever larger bodies (Safronov 1969; Dominik et al. 2007). Accumulation of differentiated meteorite parent bodies must occur while ²⁶Al and ⁶⁰Fe are still present in the solar nebula, constraining their formation time to at most a million years after the formation of calcium-aluminium-rich inclusions (Bizzarro et al. 2005; Yang, Goldstein, & Scott 2007). This coincides with the gaseous solar nebula epoch and indicates that planetesimals and protoplanets of several hundred kilometres in size were accumulated in a dense gaseous environment.

The alignment between the orbits of the planets and the rotation of the Sun is one of the key pieces of evidence for the nebular hypothesis of the formation of the solar system. The large majority of satellites also orbit their host planet in what is termed the prograde direction, i.e. orbit in the same direction as the planet orbits the sun, suggesting that they formed in circumplanetary discs. This regularity seems to extend to the predominantly prograde rotations of the planets and the largest asteroids. While the gas giant planets have likely been spun up by gas accretion, growth of solid planetary bodies by accretion of km-sized planetes-

imals is not generally expected to lead to systematic prograde rotation. Post-accretion, giant impacts which can significantly change the obliquity and spin rate of protoplanets (Dones & Tremaine 1993; Kokubo & Ida 2007) do so in a stochastic way yielding no preference for prograde motion. Successful attempts to explain a *systematic* prograde contribution from accretion of solids in a gas-free medium require special surface density profiles (Lissauer & Kary 1991) or “semicollisional” accretion (Schlichting & Sari 2007), i.e. collisions between small particles and subsequent accretion into a prograde circumplanetary particle disc that feeds the central object.

In this paper we show that prograde rotation may be a natural consequence of planetesimal growth from accretion of cm-sized solids in a gaseous environment. Providing a physical mechanism for prograde rotation in turn supports that the dominance of prograde rotation among the largest asteroids is significant despite their low number. Our model assumes simultaneous presence of cm-sized “pebbles” and gas. Such conditions are supported by observations of protoplanetary discs, which show evidence of dust growth to at least a few cm (Testi et al. 2003; Sicilia-Aguilar et al. 2007). The inferred population of mm-cm pebbles can be very substantial, on the order of 10^{-3} solar masses (Wilner et al. 2005).

We present hydrodynamical computer simulations of

* E-mail: ajohan@strw.leidenuniv.nl

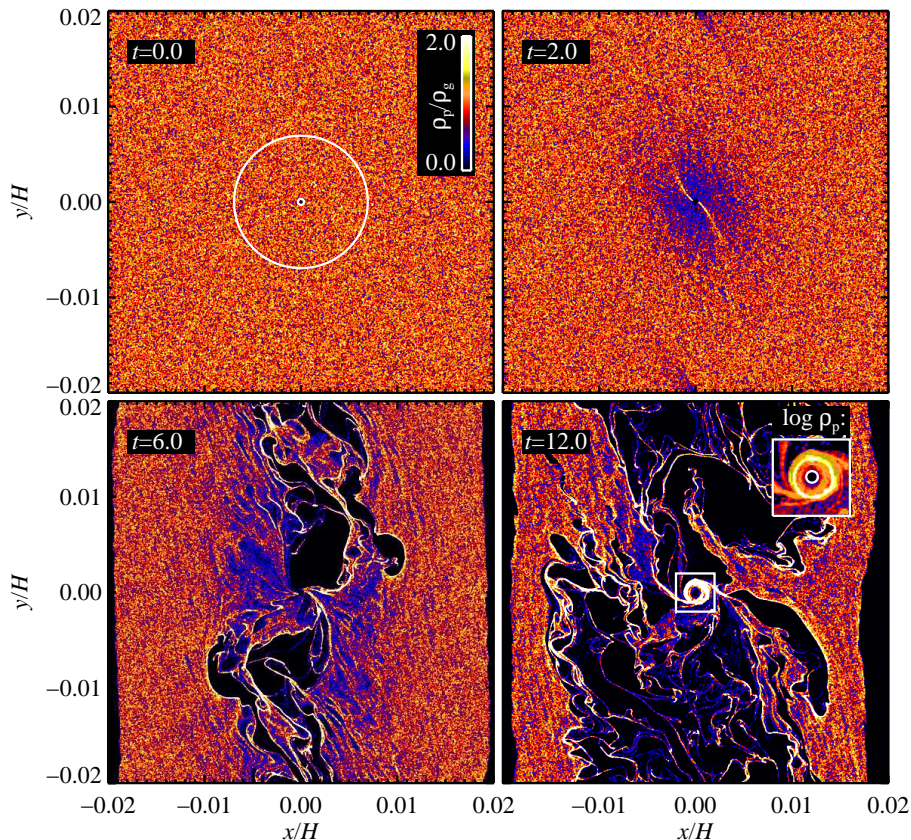


Figure 1. Accretion of pebbles onto a protoplanet fixed in the centre of the coordinate system. The first panel indicates the Hill radius and the accretion radius (inner hole). The colour coding shows the local density of solids, in units of the mid-plane gas density. Particles are initially accreted from the second and fourth quadrants (second panel). As pebble streams drag the gas down towards the protoplanet, the incompressible gas expands in great particle-free bubbles, eventually making the system turbulent (third panel). A prograde accretion disc, fed from the second and fourth quadrants, forms around the protoplanet (fourth panel).

the accretion of pebbles and rocks onto young protoplanets in a gaseous nebula environment. We find that particle streams interacting with the gas far out within the Hill sphere dissipate enough energy that the particles spiral down towards the protoplanet and form a prograde accretion disc. The prograde motion is transferred to protoplanet rotation as the particles are accreted. To explain the observed rotations of the largest asteroids and Kuiper belt objects, we propose that protoplanets accreted a major fraction (10%–50%) of their mass from pebbles and rocks during the gaseous solar nebula phase.

The paper is organised as follows. In §2 we describe the set up of our simulations. In §3 the main results are presented, both for 2-D and 3-D simulations. We speculate in §4 about implications for the observed prograde rotation of large asteroids and the future prospect of measuring rotation directions of Kuiper belt objects. We conclude on our findings in §5. The appendices contain details that do not appear in the main paper and several tests of the validity of our results. In Appendix A the dynamical equations are presented. We validate the code in Appendix B against known results on the accreted angular momentum. Appendix C describes drag forces in more detail and also the translation from dimensionless friction time to physical particle size. In Appendix D we compare time-scales of drag force and

particle collisions and conclude that drag forces are by far the dominant force, except in regions that are highly particle dominated. In Appendix E we present results at lower and higher resolution and conclude that prograde rotation is strengthened with increasing resolution. The dependence of the results on the size of the simulation box are treated in Appendix F.

2 SIMULATION SET UP

We perform numerical simulations of the coupled motion of solids and gas in a local coordinate frame corotating with the disc at the Keplerian frequency Ω_K at an arbitrary distance r_0 from the central star (Goldreich & Tremaine 1980). Coordinate axes are oriented such that x points radially away from the star and y points along the rotation direction of the disc. Particles are treated by a Lagrangian method, interacting with the gas through two-way drag forces operating on the friction time-scale τ_f . An additional gravitational force contribution from a protoplanet of mass M_p fixed in the centre of the coordinate frame is added. The gas is evolved on a fixed grid and also feels the gravity of the protoplanet (see Appendix A for details on the dynamical equations). In Appendix B we validate the results of the code against known

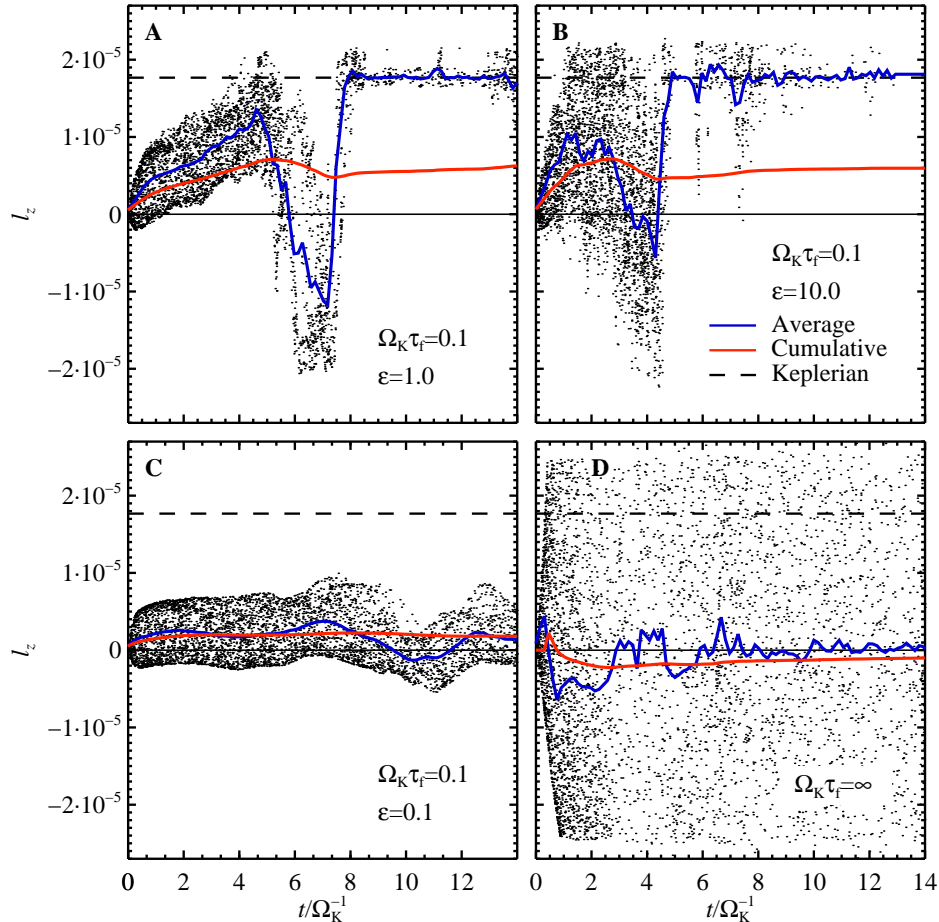


Figure 2. Delivery of prograde angular momentum to a protoplanet of 400 km radius (if placed at $r_0 = 10$ AU). The dots show the angular momentum of a subset of the accreted particles, while the blue (black) and red (grey) lines indicate the instantaneous and cumulative average. (A–B) Accretion of pebbles from environment with mean solids-to-gas ratio $\epsilon = 1.0$ and $\epsilon = 10.0$, respectively. The presence of a Keplerian particle disc is clearly visible at late times where the accreted angular momentum is exactly equal to that of a Keplerian disc (dashed line). (C) In the low solids-to-gas ratio case ($\epsilon = 0.1$) the pebbles have little influence on the gas and their motion is strongly damped as they approach the protoplanet, imparting only little rotation to the protoplanet. (D) Without drag forces these effectively very large particles give a net retrograde rotation to the protoplanet.

results on angular momentum accretion (Schlichting & Sari 2007).

Momentum conservation in the two-way drag force coupling between solid particles and gas is assured by assigning the drag force added on a particle back to the gas with the opposite sign by a second order scheme. This drag force scheme has been shown to successfully reproduce the linear growth rate of streaming instabilities in protoplanetary discs (Youdin & Johansen 2007).

We integrate the dynamical equations of particles and gas using the high order finite difference code Pencil Code (Brandenburg 2003). To avoid underresolution of motion near the protoplanet, we always freeze the gas inside a ring of diameter eight grid points around the protoplanet. Particles crossing that ring are considered to be accreted onto the protoplanet.

The Hill radius, $R_H = (GM_p/3\Omega_K^2)^{1/3}$ where G is the gravity constant, bounds the region where the gravity of the protoplanet dominates over the tidal force from the star. In a protoplanetary disc with vertical pressure scale height

H , a protoplanet with mass $GM_p = 10^{-6}\Omega_K^2 H^3$ has $R_H \approx 0.007H$. At $r_0 = 10$ AU, with disc aspect ratio $H/r_0 = 0.06$, the protoplanet has mass $M_p \approx 4 \times 10^{23}$ g and radius $R_p \approx 400$ km. At $r = 3$ AU (disc aspect ratio $H/r_0 = 0.043$) the protoplanet mass would be $M_p \approx 1.6 \times 10^{23}$ g and its radius $R_p \approx 290$ km.

We use a standard box size of $(L_x, L_y) = (0.04H, 0.04H)$, at a standard resolution of 512^2 grid points and 10^6 particles. This gives a resolution element of around 5,000 kilometres, making the inner cavity 20,000 kilometres in radius at the standard resolution. In Appendix E we present 256^2 and 1024^2 simulations. The inner cavity corresponds to 1/10, 1/20 and 1/40 of the Hill radius for low, medium and high resolution studies, respectively. The convergence test in Appendix E shows that the prograde rotation is strengthened at higher resolution with a correspondingly smaller inner accretion radius.

3 RESULTS

In Figure 1 we show results of a simulation with an assumed solids-to-gas ratio ϵ of unity (mimicking conditions in a sedimentary mid-plane layer) and a friction time $\Omega_K \tau_f = 0.1$ (relative to the inverse Keplerian orbital frequency). This friction time represents particles of a few cm in radius (Weidenschilling 1977a). See Appendix C for details. The total mass of particles in the simulation domain is approximately 1.8×10^{22} g at $r = 3$ AU (with particle column density $\Sigma_p = 3$ g cm $^{-2}$) and 6.4×10^{22} g at $r = 10$ AU (with $\Sigma_p = 0.5$ g cm $^{-2}$).

As time progresses a spiral density wave structure appears inside the Hill sphere. Particles are accreted primarily from the second and fourth quadrants. As the particles drag the gas along towards the protoplanet surface, and the gas is nearly incompressible, the gas leaves through a “wind” in the first and third quadrants. This wind prevents particles from entering from these sides.

Later in the simulation the particle-gas layer becomes turbulent, due to the bubbles of gas expanding from the protoplanet surface. A prograde particle disc forms around the protoplanet, still fed from the second and fourth quadrants. This disc is completely dominated by particles ($\rho_p/\rho_g \gg 10$) and accretes slowly, due to stirring by the turbulent surroundings. We show in Appendix D that while particle collisions are negligible in most of the simulation domain, collisions will dominate over gas drag in the circumplanetary disc. However, we do not model the collisional viscosity in the presented simulations, as we wish to keep the system as simple as possible. A numerical algorithm for treating collisions between superparticles is currently under development (Johansen, Lithwick, & Youdin, in preparation).

In Figure 2 we plot the angular momentum of accreted particles as a function of time, for a subset of randomly sampled particles. Initially, during the spiral density wave phase, there is a preference for accreting prograde particles. This is normally followed by a short phase of retrograde accretion, where a retrograde accretion disc may temporarily form. Eventually the particles always enter a prograde accretion disc, and the protoplanet accretes the full Keplerian surface frequency.

Convergence tests are presented in Appendix E. Both lower and higher resolution studies result in a similar amount of prograde accretion, although there is a trend for accreting stronger prograde rotation with increasing resolution. In Appendix F we present results for a box size of $0.1H \times 0.1H$. The larger box size has a net positive effect on the prograde rotation of the protoplanet. The sign of the angular momentum is more consistently positive than in the small box, and there are fewer periods of retrograde accretion.

3.1 Dependence on particle size

It was shown analytically by Muto & Inutsuka (2008) that particles approaching the protoplanet feel the opposing effects of protoplanet gravity (at large distances) and gravitational scattering (at short distances). For particles with $\Omega_K \tau_f < 1$, drag forces are so strong that particles are accreted into the Hill sphere, while larger particles are scattered by the planet and only approach the protoplanet to

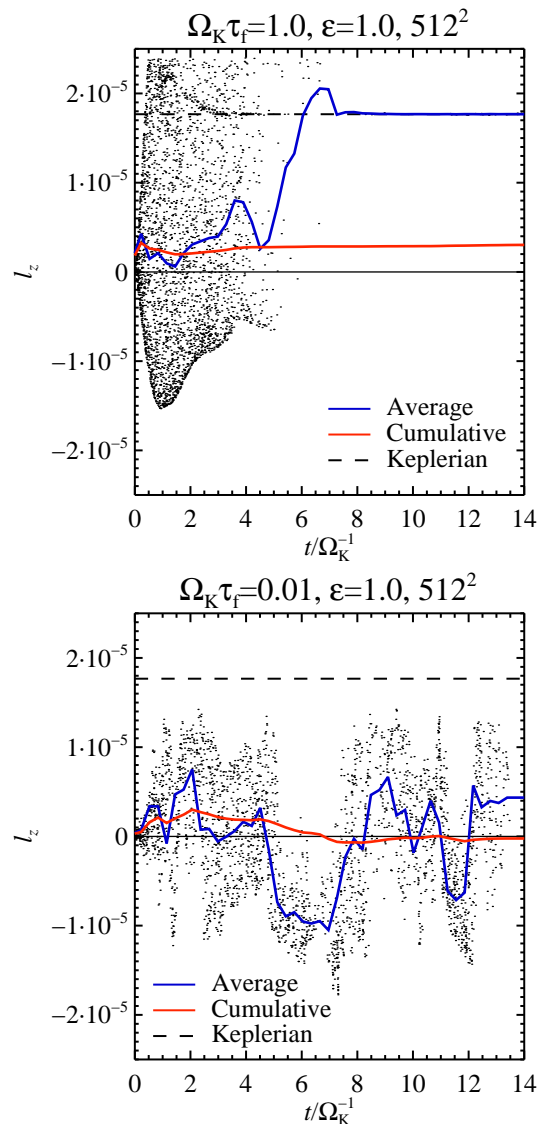


Figure 3. Accretion of larger and smaller particles. Marginally coupled particles $\Omega_K \tau_f = 1$ particles (top plot) readily form a prograde particle disc. The particles are much less affected by the gas than the particles presented in Fig. 2, thus the particle disc accretes very slowly. Smaller particles with $\Omega_K \tau_f = 0.01$, corresponding to sizes of a few mm, are so coupled to the gas that accretion takes place as a sedimentation towards the protoplanet, with a significant loss of angular momentum to the gas (bottom plot).

some minimum distance. Similarly Weidenschilling & Davis (1985) showed that planetesimals above a certain size are trapped in mean motion resonances with growing planets. This shepherding might affect boulders of sizes metres to ten metres.

In Fig. 3 we show the accretion of larger, $\Omega_K \tau_f = 1$, and smaller, $\Omega_K \tau_f = 0.01$, particles, corresponding to a few metres and a few millimetres, respectively. The larger particles readily form a prograde particle disc around the protoplanet. However, the marginal coupling to the gas makes the particle disc much more stable to dynamical shaking by the surrounding gas, and the disc only accretes slowly. Smaller

particles, on the other hand, are very coupled to the gas, and accretion takes place as a slow sedimentation. The particles lose a significant fraction of their angular momentum to the gas and arrive almost perpendicular to the protoplanet surface.

Thus we can put a relatively tight constraint on the particle sizes that can lead to prograde rotation of protoplanets. A dimensionless friction time between approximately 0.1 and 1.0 corresponds to particles of radii between a few cm and a few ten cm. However, at several ten AU from the central star, where the gas column density drops to $\Sigma_g \approx 5 \text{ g cm}^{-2}$, the “good” particle sizes are between a few mm and a few cm, approximately corresponding to the pebbles that are observed in the outer regions of protoplanetary discs (Testi et al. 2003; Wilner et al. 2005; Rodmann et al. 2006; Lommen et al. 2009).

3.2 Sub-Keplerian motion

An additional effect that we have not considered so far is the sub-Keplerian motion of the gas. As the gas is slightly pressure supported in the radial direction, the gas orbital motion is slower (by approximately 5% of the sound speed or 0.5% of the Keplerian speed) than the Keplerian value (Adachi, Hayashi, & Nakazawa 1976; Weidenschilling 1977a). Isolated particles face a constant headwind of the gas, causing them to orbit slower and to drift radially. The stationary protoplanet is thus exposed to a “sandblast” with velocity $\sim 25 \text{ m s}^{-1}$. In Fig. 4 we consider a simulation of $\Omega_K \tau_f = 0.1$ particles with an initial solids-to-gas ratio of 10. The strong mass loading of particles reduces the head wind significantly in the beginning, and we observe the usual prograde accretion. However, as the particles lose influence on the gas, a sandblasting phase occurs in which no net rotation is induced on the protoplanet. Overall the protoplanet nevertheless accretes a significant fraction of the Keplerian surface frequency.

3.3 3-D results

For simplicity, and to obtain higher resolution and smaller accretion radius, we have so far presented results of 2-D simulations. In this section we show that we obtain similar results in 3-D as in 2-D. We ignore the effect of vertical gravity and stratification on the gas, a small effect in boxes with a vertical extent of $L_z/2 = 0.02H$. We initialize the particles with a Gaussian density distribution around the mid-plane, of scale height $H_p = 0.01H$, and a column density of 0.01 relative to the gas. The results of a 3-D simulation with 256^3 grid points and 8×10^6 particles are shown in Fig. 5. The particles show the usual strong preference for prograde accretion. A prograde accretion disc also forms around the protoplanet in the 3-D simulation (see Fig. 6), but this is not as evident from the accreted angular momentum as in 2-D because isolated particles, now entering from all directions, are accreted faster than the disc material. We conclude that our assumption of 2-D flow represents the true 3-D physical behaviour of the system well. The 2-D assumption, at the same time, allows for much higher resolution investigations and a higher particle number per grid cell.

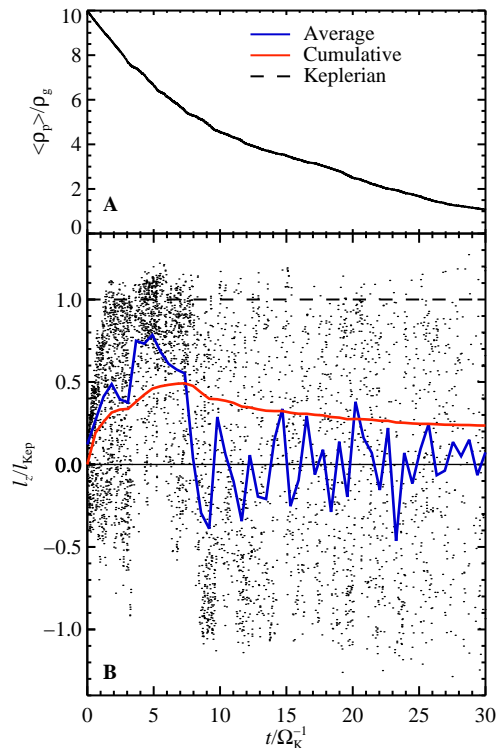


Figure 4. Sandblasting a protoplanet with pebbles. (A) Mean particle density in the box as a function of time, (B) the accreted angular momentum. At the initial solids-to-gas ratio of 10, a net positive angular momentum is accreted by the protoplanet. But as the particles are accreted, the remaining particles drift stronger and stronger relative to the protoplanet, eventually leading to ballistic accretion with no net angular momentum.

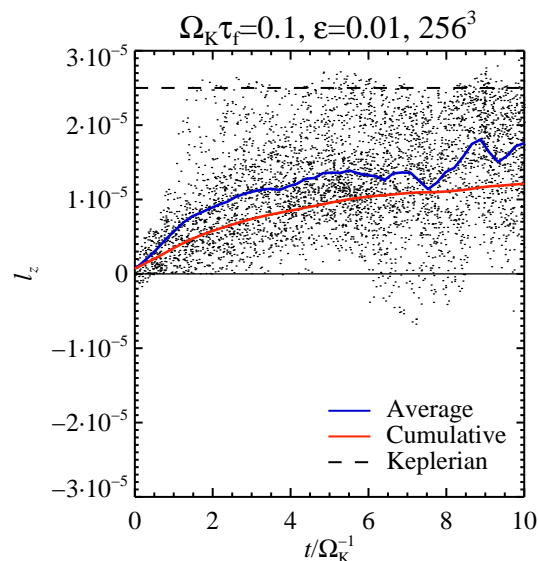


Figure 5. 3-D accretion. The 3-D simulation has resolution $N_x = N_y = N_z = 256$ and $N_p = 8 \times 10^6$. We recover the usual preference for prograde accretion, showing that the higher resolution 2-D simulations presented in the Fig. 2 represent the physical system well.

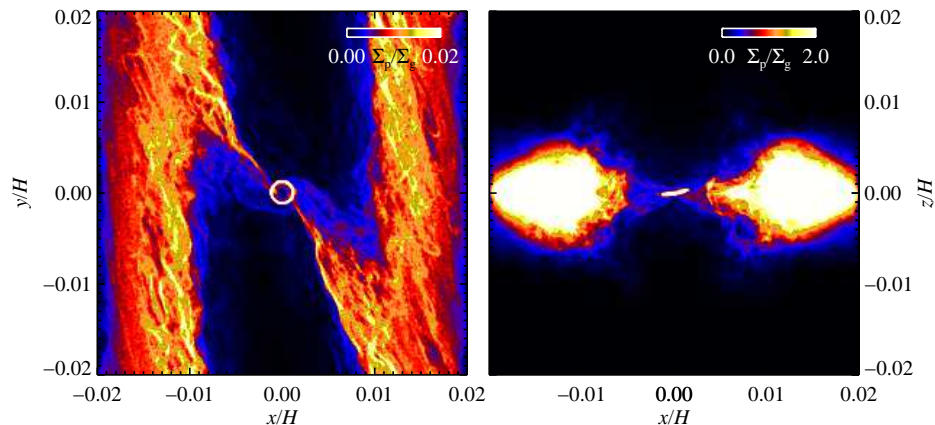


Figure 6. 3-D structure. The figure shows the column density of particles in the x - y plane (left panel) and in the x - z plane (right panel). The column density has been normalized by the gas column density in the relevant direction. A thin particle disc orbits close to the protoplanet, surrounded by the thicker particle mid-plane layer outside the Hill sphere.

4 DISCUSSION

4.1 Prograde rotation in the solar system

The asteroid belt is a collisionally evolved collection of rocky and icy bodies residing roughly between the orbits of Mars and Jupiter. Analytical and numerical studies indicate that the largest asteroids have not suffered enough collisional evolution to significantly alter their spin vector (McAdoo & Burns 1973; Farinella et al. 1992). These objects have thus likely retained their primordial spin angular momentum and may be representative of the original protoplanet population (see also Morbidelli et al. 2009). Figure 7 depicts a collection of spin axis obliquities of 62 asteroids larger than 50 km in diameter (from Kryszczyńska et al. 2007). The obliquity is here defined as the angle between the pole vector of an asteroid and the normal to the ecliptic plane. While smaller asteroids have collisionally randomized obliquities, the largest ones ($r > 150$ km) display a propensity towards prograde rotation (obliquity $< 90^\circ$), i.e. rotation in the same direction as the orbit. Indeed, the two most massive asteroids, Ceres and Vesta, spin progradely with obliquities of 9° and 36° and periods 9.1 and 5.3 hours. If their spin orientations were collisionally randomized, the probability that their mean obliquity is less than the observed value is only $p \sim 2.5 \times 10^{-3}$ (3σ). In Fig. 8 we show the mean pole angle (relative to the ecliptic) of asteroids as a function of their size. There is a trend towards prograde rotation for all size ranges, although the statistical significance is only 1–2 σ .

The Kuiper belt, a dynamically stable region beyond Neptune, preserves roughly a dozen known 1000 km-scale icy bodies (Jewitt 1999; Chiang et al. 2007; Brown 2008). As in the case of asteroids, collisional evolution simulations of Kuiper belt objects (KBOs) show that bodies larger than $r \approx 200$ km have sustained relatively mild collisional evolution (Davis & Farinella 1997) and their primordial spins have survived the random effect of impacts for the age of the solar system (Lacerda 2005). No KBO obliquities have been derived as the known objects have moved less than 30° along their orbits since discovery, but several rotation periods have been measured (Fig. 9). With the ex-

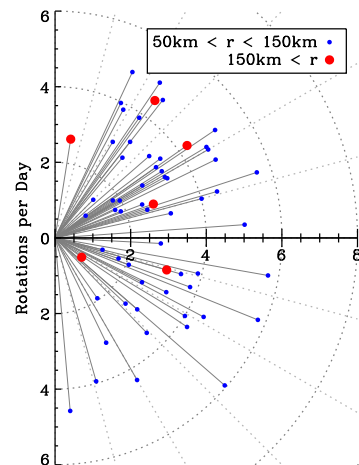


Figure 7. Obliquity of asteroids larger than 50 km in radius with respect to the ecliptic plane (x -axis). Each asteroid is represented by a blue (black) dot, connected to the origin by a grey line. The angle between each grey line and the positive y -axis is the obliquity of the corresponding asteroid. The length of the lines gives the spin frequency of the asteroid in rotations per day. Asteroids in the upper quadrant are prograde and asteroids in the lower quadrant are retrograde. Asteroids larger than $r = 150$ km, represented by larger, red (dark grey) dots, show a preference for prograde rotation.

ception of Pluto and Haumea, both believed to have suffered massive collisions (Canup 2005; Brown et al. 2007), the rotation periods of KBOs larger than $r = 200$ km lie in a narrow 5 to 20 hour range (Lacerda & Luu 2006; Sheppard, Lacerda, & Ortiz 2008). The same is true for Ceres and the other three asteroids in the same size range, which have orbital timescales one to two orders of magnitude shorter than KBOs. Such uniformity in spin period for bodies with different compositions and presumably formed and evolved at very different heliocentric distances suggests a common spin-up mechanism.

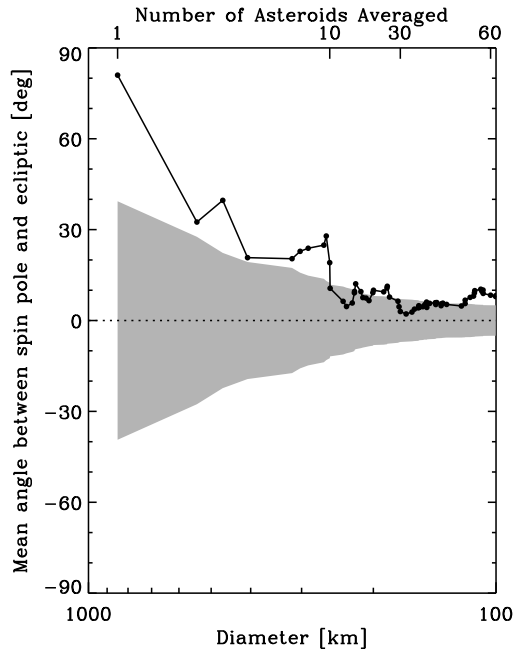


Figure 8. Mean pole angle of asteroids as a function of their size in kilometres. The black dots show the cumulative mean angle from the ecliptic. We connect the dots with a line to guide the eye. The first dot from the left is the pole angle of Ceres. The second dot is the mean of Ceres and Pallas, and so on. The shaded region is the $1\text{-}\sigma$ region expected from random spin orientations. The line is above the grey area until approximately the 10th largest asteroid, although low significance prograde rotation persists even for smaller asteroids.

4.2 Spin-up of protoplanets

The numerical experiments presented in §3 show that accretion of particle sizes of a few cm to a few m and a solids-to-gas ratio around unity or higher (see Figure 3) leads to a systematic prograde rotation of protoplanets, in agreement with the observed trend in the largest asteroids. This moderately high solids-to-gas ratio points to the sedimentary mid-plane, or to dense particle clumps appearing in such a mid-plane layer (Johansen et al. 2007; Cuzzi, Hogan, & Shariff 2008), as a prime site for the growth of protoplanets. The evaporation of gas by irradiation from the central star or neighbouring O stars leads to a similar increase in the influence of the dust particles on the gas (Throop & Bally 2005; Alexander & Armitage 2007; Johansen, Youdin, & Mac Low 2009).

Our simulations predict that the largest Kuiper belt objects should preferentially rotate in the prograde direction around their axis. A few exceptions to this trend are objects that have suffered massive impacts (e.g. Haumea, Brown et al. 2007).

Pure accretion from a circumplanetary disc would lead to a protoplanet rotation period of only a few hours, near the centrifugal break up speed. However, accretion from a circumplanetary disc need not be the only mass source. Growth phases with little or no accreted angular momentum can occur when the protoplanet accretes isolated dust particles and pebbles or km-sized planetesimals or other protoplanets. Protoplanets thus need to obtain between 10% and 50%

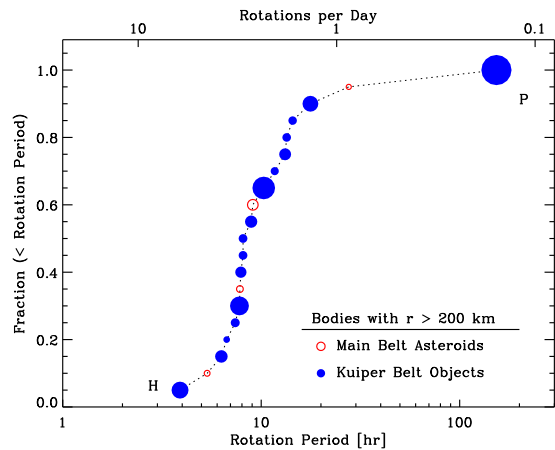


Figure 9. Cumulative spin period distribution of Kuiper belt objects and asteroids larger than 200 km in radius. Most objects lie in a narrow $5 < P < 20$ hour period range irrespective of their other physical properties. Outliers Haumea (H) and Pluto (P) are marked; they are believed to have suffered massive collisions.

of their mass from the accretion of macroscopic dust particles in a gaseous environment. The lower limit is relevant if all pebbles are accreted at the full Keplerian angular momentum, while the upper limit is relevant if 80% of the mass accretion occurs through pebble sandblasting or through accretion of “planetesimals” with high τ_f .

The sub-Keplerian sandblasting effect described in §3.2 means that the mechanism for obtaining prograde rotation works best in particle-dominated flows or in regions of low radial drift. The radial drift can be reduced or even reversed in persistent pressure bumps appearing in the gas (Haghighipour & Boss 2003). Recent studies have shown how planetesimal formation by self-gravity (Johansen et al. 2007; Kato et al. 2009) and by coagulation (Kretke & Lin 2007; Brauer, Henning, & Dullemond 2008) proceed in such convergence regions in the flow of solid particles.

4.3 Spin-up in absence of gas?

It was recently proposed by Schlichting & Sari (2007) that inelastic particle collisions will lead to accretion of prograde rotation from a circumplanetary particle disc during the gas-free stages of planetary growth. Such a mechanism may be able to provide additional prograde angular momentum after the giant impact stage. This is especially relevant for the terrestrial planets which are believed to have been accumulated over 10-100 million years in a gas free environment (Lunine et al. 2010). Mercury, Earth and Mars all have prograde spins, but the spins of the terrestrial planets have been substantially modified by long-term perturbations by other planets (Laskar & Robutel 1993).

Focusing instead on the largest asteroids and Kuiper belt objects, our numerical simulations show that pebbles and rocks are accreted very efficiently by the protoplanets. In the main numerical simulation presented in §3 the protoplanet+disc system accretes 1/7 of the protoplanet mass in five orbits (≈ 25 years at 3 AU). Such high accretion rates are facilitated by the presence of gas in the Hill sphere. This indicates that young protoplanets can accrete lots of mate-

rial already during the protoplanetary gas disc phase. The actual ratio of accretion during and after the gaseous disc phase is nevertheless relatively unconstrained and deserves further attention in the future.

5 CONCLUSIONS

We present computer simulations of the accretion of pebbles and rocks onto young protoplanets in a gaseous nebula environment. Our findings can be summarised as follows:

- Particle streams interacting with the gas far out in the Hill sphere of the growing protoplanet dissipate enough energy that the particles spiral down towards the central object and form a prograde accretion disc. The prograde motion is transferred to the protoplanet as the particles are accreted.
- In order to explain the observed rotations of the largest asteroids and Kuiper belt objects, we propose that protoplanets accreted a major fraction (10%–50%) of their mass from pebbles and rocks during the gaseous solar nebula phase.
- A specific prediction of our model is that most of the largest Kuiper belt objects should possess prograde spins.

Since the Keplerian surface frequency depends only on the density of the protoplanet, accretion from a Keplerian particle disc explains how asteroids and Kuiper belt objects can have similar rotation periods even though the orbital time-scale is much longer in the Kuiper belt. Our results imply not just a universality in the rotation period of solid bodies in the solar system, but also in the formation process and in the important role of gas and pebbles for the growth of hundred kilometre scale protoplanets.

Future numerical work should focus on the extension of the presented model to include turbulence driven by global instabilities and more realistic solid physics, such as a distribution of particle sizes, collisional viscosity and collisional fragmentation.

ACKNOWLEDGMENTS

Computer simulations were performed at the PIA cluster of the Max Planck Institute for Astronomy. PL is grateful for the support of a Royal Society Newton Fellowship. The authors would like to thank Hilke Schlichting for reading and commenting an early version of the manuscript.

REFERENCES

- Adachi I., Hayashi C., Nakazawa K., 1976, *Progress of Theoretical Physics*, 56, 1756
- Alexander R. D., Armitage P. J., 2007, *MNRAS*, 375, 500
- Balbus S. A., Hawley J. F., 1998, *Reviews of Modern Physics*, 70, 1
- Bizzarro M., Baker J. A., Haack H., Lundgaard K. L., 2005, *ApJ*, 632, L41
- Brandenburg A., 2003, *Computational aspects of astrophysical MHD and turbulence (Advances in Nonlinear Dynamics)*, 269
- Brauer F., Henning T., Dullemond C. P., 2008, *A&A*, 487, L1
- Brown M. E., 2008, *The Largest Kuiper Belt Objects*, ed. M. A. Barucci, H. Boehnhardt, D. P. Cruikshank, & A. Morbidelli, 335
- Brown M. E., Barkume K. M., Ragozzine D., Schaller E. L., 2007, *Nature*, 446, 294
- Canup R. M., 2005, *Science*, 307, 546
- Chiang E., Lithwick Y., Murray-Clay R., Buie M., Grundy W., Holman M., 2007, in *Protostars and Planets V*, ed. B. Reipurth, D. Jewitt, K. Keil, 895
- Cuzzi J. N., Dobrovolskis A. R., Champney J. M., 1993, *Icarus*, 106, 102
- Cuzzi J. N., Hogan R. C., Shariff K., 2008, *ApJ*, 687, 1432
- Davis, D. R., & Farinella P., 1997, *Icarus*, 125, 50
- Dominik C., Blum J., Cuzzi J. N., Wurm G., 2007, in *Protostars and Planets V*, ed. B. Reipurth, D. Jewitt, K. Keil, 783
- Dones L., Tremaine S., 1993, *Icarus*, 103, 67
- Dones L., Tremaine S., 1993, *Science*, 259, 350
- Farinella P., Davis D. R., Paolicchi P., Cellino A., Zappala V., 1992, *A&A*, 253, 604
- Goldreich P., Tremaine S., 1980, *ApJ*, 241, 425
- Haghighipour N., Boss A. P., 2003, *ApJ*, 583, 996
- Hayashi C., 1981, *Prog. Theor. Phys.*, 70, 35
- Jewitt D., 1999, *Annual Review of Earth and Planetary Sciences*, 27, 287
- Johansen A., Oishi J. S., Mac Low M.-M., Klahr H., Henning T., Youdin A., 2007, *Nature*, 448, 1022
- Johansen, A., Youdin, A., & Mac Low, M. 2009, *ApJ*, 704, L75
- Kato M. T., Nakamura K., Tandokoro R., Fujimoto M., Ida S., 2009, *ApJ*, 691, 1697
- Kokubo E., Ida S., 2007, *ApJ*, 671, 2082
- Kretke K. A., Lin D. N. C., 2007, *ApJ*, 664, L55
- Kryszczyńska A., La Spina A., Paolicchi P., Harris A. W., Breiter S., Pravec P., 2007, *Icarus*, 192, 223
- Lacerda P., 2005, PhD thesis, Leiden University, <https://openaccess.leidenuniv.nl/handle/1887/603>
- Lacerda P., Luu J., 2006, *AJ*, 131, 2314
- Laskar J., Robutel P., 1993, *Nature*, 361, 608
- Lissauer J. J., Kary D. M., 1991, *Icarus*, 94, 126
- Lommen, D., Maddison, S. T., Wright, C. M., van Dishoeck, E. F., Wilner, D. J., & Bourke, T. L. 2009, *A&A*, 495, 869
- Lunine, J. I., O'Brien, D. P., Raymond, S. N., Morbidelli, A., Quinn, T., & Graps, A. 2010, *Advanced Science Letters*, in press (arXiv:0906.4369)
- Machida M. N., Kokubo E., Inutsuka S.-i., Matsumoto T., 2008, *ApJ*, 685, 1220
- McAdoo D. C., Burns J. A., 1973, *Icarus*, 18, 285
- Morbidelli, A., Bottke, W. F., Nesvorný, D., & Levison, H. F. 2009, *Icarus*, 204, 558
- Muto T., Inutsuka S.-i., 2009, *ApJ*, 695, 1132
- Nakagawa Y., Sekiya M., Hayashi C., 1986, *Icarus*, 67, 375
- Rodmann, J., Henning, T., Chandler, C. J., Mundy, L. G., & Wilner, D. J. 2006, *A&A*, 446, 211
- Safronov V. S., 1969, *Evolution of the protoplanetary cloud and formation of Earth and the planets (Jerusalem: Israel Sci. Transl.)*
- Schlichting H. E., Sari R., 2007, *ApJ*, 658, 593
- Sheppard S. S., Lacerda P., Ortiz J. L., 2008, *Photometric Lightcurves of Transneptunian Objects and Centaurs: Rotations, Shapes, and Densities*, ed. M. A. Barucci,

H. Boehnhardt, D. P. Cruikshank, A. Morbidelli, 129
 Sicilia-Aguilar A., Hartmann L. W., Watson D., Bohac C.,
 Henning Th., Bouwman J., 2007, ApJ, 659, 1637
 Testi L., Natta A., Shepherd D. S., Wilner D. J., 2003,
 A&A, 403, 323
 Throop H. B., Bally J., 2005, ApJ, 623, L149
 Weidenschilling S. J., 1977a, MNRAS, 180, 57
 Weidenschilling S. J., 1977b, Ap&SS, 51, 153
 Weidenschilling S. J., Davis D. R. 1985, Icarus, 62, 16
 Wilner D. J., D'Alessio P., Calvet N., Claussen M. J., Hart-
 mann L., 2005, ApJ, 626, L109
 Yang J., Goldstein J. I., Scott E. R. D., 2007, Nature, 446,
 888
 Youdin A., Johansen A., 2007, ApJ, 662, 613

APPENDIX A: DYNAMICAL EQUATIONS

We simulate the coupled motion of particles and gas in the shearing sheet frame (Goldreich & Tremaine 1980). The frame rotates at the Keplerian frequency Ω_K at an arbitrary distance r_0 from the central star. Axes are oriented such that x points radially away from the star, y points along the rotation direction of the disc, while z points vertically out of the orbital plane. The particle component is treated as Lagrangian particles, each with a position vector $\mathbf{x} = (x, y)$ and a velocity vector $\mathbf{v} = (v_x, v_y)$, with dynamical equations

$$\dot{x} = v_x, \quad (\text{A1})$$

$$\dot{y} = v_y - (3/2)\Omega_K x, \quad (\text{A2})$$

$$\dot{v}_x = +2\Omega_K v_y - \frac{GM_p x}{(x^2 + y^2)^{3/2}} - \frac{1}{\tau_f}(v_x - \bar{u}_x), \quad (\text{A3})$$

$$\dot{v}_y = -\frac{1}{2}\Omega_K v_x - \frac{GM_p y}{(x^2 + y^2)^{3/2}} - \frac{1}{\tau_f}(v_y - \bar{u}_y). \quad (\text{A4})$$

We measure the velocity in the y -direction relative to the linearised Keplerian shear $u_y^{(0)} = -(3/2)\Omega_K x$, which gives rise to a change in the Coriolis force appearing in equation (A4). An additional force contribution from the protoplanet of mass M_p fixed in the centre of the coordinate frame is added. We also consider the drag force from the gas, acting on the friction time-scale τ_f and proportional to the velocity difference between particles and gas. The gas velocity $\bar{\mathbf{u}} = (\bar{u}_x, \bar{u}_y)$ at the position of a particle is found by spline interpolation from the nearest three grid points in each direction (Youdin & Johansen 2007).

The evolution of gas is solved on a fixed Cartesian grid. The equations of motion for the gas velocity field \mathbf{u} , relative to the Keplerian shear, and the continuity equation for gas density ρ_g , read

$$\frac{\partial u_x}{\partial t} + (\mathbf{u} \cdot \nabla)u_x + u_y^{(0)} \frac{\partial u_x}{\partial y} = +2\Omega_K u_y - 2\Omega_K \Delta v - \frac{GM_p x}{(x^2 + y^2)^{3/2}} - c_s^2 \frac{\partial \ln \rho_g}{\partial x} - \frac{\epsilon}{\tau_f}(u_x - \bar{v}_x), \quad (\text{A5})$$

$$\frac{\partial u_y}{\partial t} + (\mathbf{u} \cdot \nabla)u_y + u_y^{(0)} \frac{\partial u_y}{\partial y} = -\frac{1}{2}\Omega_K u_x - \frac{GM_p y}{(x^2 + y^2)^{3/2}} - c_s^2 \frac{\partial \ln \rho_g}{\partial y} - \frac{\epsilon}{\tau_f}(u_y - \bar{v}_y), \quad (\text{A6})$$

$$\frac{\partial \rho_g}{\partial t} + (\mathbf{u} \cdot \nabla)\rho_g + u_y^{(0)} \frac{\partial \rho_g}{\partial y} = -\rho_g \nabla \cdot \mathbf{u}. \quad (\text{A7})$$

In equation (A5) we include the possibility of adding a radial pressure gradient $\partial \ln P / \partial \ln r$ through the sub-Keplerian velocity

$$\Delta v = -\frac{1}{2} \frac{H}{r} \frac{\partial \ln P}{\partial \ln r} c_s. \quad (\text{A8})$$

We use $\Delta v = 0$ except in §3.2 where we set $\Delta v = 0.05c_s$ (Nakagawa, Sekiya, & Hayashi 1986). The gas also feels the gravity of the protoplanet. For the back-reaction friction force from the particles we calculate the local solids-to-gas ratio through $\epsilon = \bar{\rho}_p / \rho_g$.

The dynamical equations for the evolution of particles and gas appear in 3-D as

$$\dot{x} = v_x, \quad (\text{A9})$$

$$\dot{y} = v_y - (3/2)\Omega_K x, \quad (\text{A10})$$

$$\dot{z} = v_z, \quad (\text{A11})$$

$$\dot{v}_x = +2\Omega_K v_y - \frac{GM_p x}{(x^2 + y^2 + z^2)^{3/2}} - \frac{1}{\tau_f}(v_x - \bar{u}_x), \quad (\text{A12})$$

$$\dot{v}_y = -\frac{1}{2}\Omega_K v_x - \frac{GM_p y}{(x^2 + y^2 + z^2)^{3/2}} - \frac{1}{\tau_f}(v_y - \bar{u}_y), \quad (\text{A13})$$

$$\dot{v}_z = -\Omega_K^2 z - \frac{GM_p z}{(x^2 + y^2 + z^2)^{3/2}} - \frac{1}{\tau_f}(v_z - \bar{u}_z), \quad (\text{A14})$$

$$\frac{\partial u_x}{\partial t} + (\mathbf{u} \cdot \nabla)u_x + u_y^{(0)} \frac{\partial u_x}{\partial y} = +2\Omega_K u_y - \frac{GM_p x}{(x^2 + y^2 + z^2)^{3/2}} - c_s^2 \frac{\partial \ln \rho_g}{\partial x} - \frac{\epsilon}{\tau_f}(u_x - \bar{v}_x), \quad (\text{A15})$$

$$\frac{\partial u_y}{\partial t} + (\mathbf{u} \cdot \nabla)u_y + u_y^{(0)} \frac{\partial u_y}{\partial y} = -\frac{1}{2}\Omega_K u_x - \frac{GM_p y}{(x^2 + y^2 + z^2)^{3/2}} - c_s^2 \frac{\partial \ln \rho_g}{\partial y} - \frac{\epsilon}{\tau_f}(u_y - \bar{v}_y), \quad (\text{A16})$$

$$\frac{\partial u_z}{\partial t} + (\mathbf{u} \cdot \nabla)u_z + u_y^{(0)} \frac{\partial u_z}{\partial y} = -\frac{GM_p z}{(x^2 + y^2 + z^2)^{3/2}} - c_s^2 \frac{\partial \ln \rho_g}{\partial z} - \frac{\epsilon}{\tau_f}(u_z - \bar{v}_z). \quad (\text{A17})$$

Here we subject particles to the vertical gravity component of the central star, but ignore the same term for the pressure-supported gas.

APPENDIX B: CODE VALIDATION

To validate the implementation of the protoplanet gravity in the shearing sheet frame, we test here the accretion of test particles against other published results (Schlichting & Sari 2007).

We consider a protoplanet of dimensionless mass $GM_p = 10^{-6} \Omega_K^2 H^3$ in a 2-D box of size $L_x = L_y = 0.04H$. Here Ω_K is the Keplerian orbital frequency, while H is the gas scale height. The Hill radius of the protoplanet is $R_H \approx 0.007H$. We place 10,000 particles randomly in the box, initially excluding particles from the region within the Hill sphere. The particle positions and velocities evolve in response to the Coriolis force, the tidal force from the central star and the gravity of the embedded protoplanet. For this test we ignore drag forces between particles and gas.

As the particle positions and velocities evolve, we track the first crossing of various distances from the protoplanet and calculate the mean specific angular momentum per particle for all the accretion shells. The results are shown in

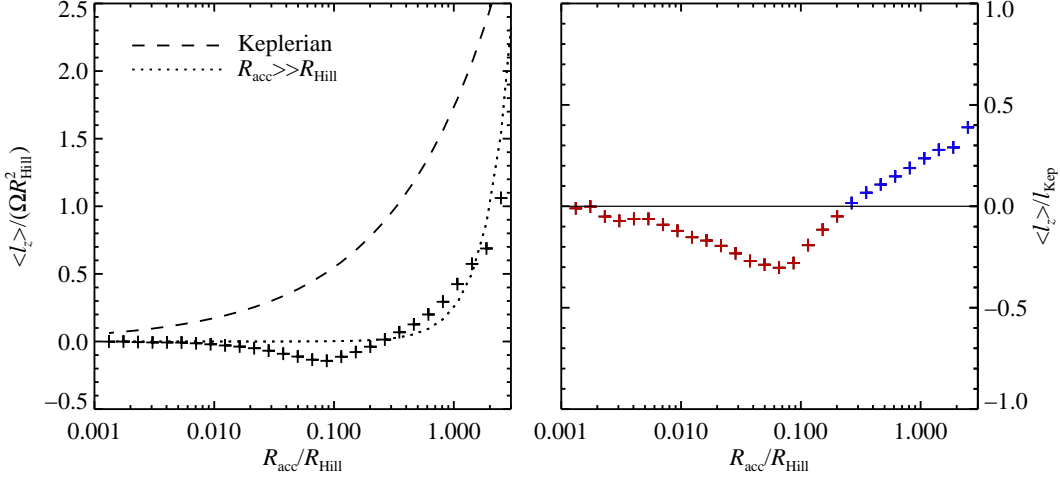


Figure A1. Code validation test. The left plot shows the mean specific angular momentum, $\langle \ell_z \rangle$, of test particles passing circles of various radius R_{acc} (x -axis). In the limit $R_{\text{acc}} \gg R_{\text{Hill}}$ the slow prograde rotation of the nebula is transferred to the “planet” [the dotted line shows the analytical expectation $\ell_z = (1/4)\Omega_K R_{\text{acc}}^2$], but particles rapidly decrease their angular momentum as they travel into the Hill sphere. The dashed line indicates prograde Keplerian specific angular momentum. The right plot shows the ratio of accreted angular momentum to the prograde Keplerian value. These non-interacting planetesimals induce a net retrograde rotation on the protoplanet. The measured angular momentum flux is in good agreement with results published in Schlichting & Sari (2007).

Fig. A1. For accretion outside of the Hill sphere, the motion is prograde, following the trend $\ell_z = (1/4)\Omega_K R_{\text{acc}}^2$ derived analytically in Dones & Tremaine (1993). However, deeper in the Hill sphere the net angular momentum is approximately zero. Particles transported to the vicinity of the protoplanet by the Keplerian shear lose their angular momentum on the way and induce slow retrograde rotation to the protoplanet. The numerical result shown in Fig. A1 is in good agreement with Schlichting & Sari (2007).

APPENDIX C: PARTICLE SIZES

We characterize particles in terms of their dimensionless friction time $\Omega_K \tau_f$ (where Ω_K is the Keplerian orbital frequency). The translation to a particle size depends on the assumed disc model. Small particles are subject to Epstein drag, valid when the particle radius is smaller than the mean free path of the gas (see below). The friction time in the Epstein regime is given by

$$\Omega_K \tau_f^{(\text{Ep})} = \frac{\Omega_K \rho_{\bullet} a}{\rho_g c_s} = \sqrt{2\pi} \frac{\rho_{\bullet} a}{\Sigma_g}, \quad (\text{C1})$$

where the second step applies in the disc mid-plane. Here ρ_{\bullet} is the material density of the solids, a is the radius of a solid body, ρ_g is the gas density, c_s is the sound speed, while Σ_g is the column density of gas. Epstein drag depends on gas density, but in practice the gas density fluctuations are negligible (order 1%) in our subsonic flows, so we ignore them. Solving for particle size gives

$$a = \frac{\Omega_K \tau_f^{(\text{Ep})} \Sigma_g}{\sqrt{2\pi} \rho_{\bullet}} \approx 60 \text{ cm } \Omega_K \tau_f^{(\text{Ep})} \left(\frac{\Sigma_g}{300 \text{ g cm}^{-2}} \right) \left(\frac{\rho_{\bullet}}{2 \text{ g cm}^{-3}} \right)^{-1}. \quad (\text{C2})$$

Applying a simulation with given τ_f values to different locations in the disc with different gas column densities changes the physical particle sizes corresponding to a given value of $\Omega_K \tau_f$. We follow the Minimum Mass Solar Nebula model (Weidenschilling 1977b; Hayashi 1981; Cuzzi, Dobrovolskis, & Champney 1993), with column density Σ_g and gas scale height H given by

$$\Sigma_g(r) = 1700 \text{ g cm}^{-2} \left(\frac{r}{\text{AU}} \right)^{-3/2}, \quad (\text{C3})$$

$$H(r) = 0.033 \text{ AU} \left(\frac{r}{\text{AU}} \right)^{5/4}. \quad (\text{C4})$$

Considering, as in the main text, $r = 3 \text{ AU}$ and $\Sigma_g = 300 \text{ g cm}^{-2}$ or $r = 10 \text{ AU}$ and $\Sigma_g = 50 \text{ g cm}^{-2}$, yields particle sizes of $a = 6 \text{ cm}$ and $a = 1 \text{ cm}$, respectively, for $\Omega_K \tau_f = 0.1$.

The Epstein regime of free molecular flow ceases to apply once the particle radius exceeds (9/4 of) the gas mean free path,

$$\lambda = \frac{\mu}{\rho_g \sigma_{\text{mol}}} = \frac{\sqrt{2\pi} \mu H}{\Sigma_g \sigma_{\text{mol}}} \quad (\text{C5})$$

$$\approx 31 \text{ cm} \left(\frac{\Sigma_g}{300 \text{ g cm}^{-2}} \right)^{-1} \left(\frac{H/r}{0.043} \right) \left(\frac{r}{3 \text{ AU}} \right), \quad (\text{C6})$$

where $\mu = 3.9 \times 10^{-24} \text{ g}$ is the mean molecular weight and $\sigma_{\text{mol}} = 2 \times 10^{-15} \text{ cm}^2$ is the molecular cross section of molecular hydrogen (Nakagawa et al. 1986). Epstein drag applies as long as

$$\Omega_K \tau_f^{(\text{Ep})} < \frac{9\pi}{2} \frac{\rho_{\bullet} \mu H}{\Sigma_g^2 \sigma_{\text{mol}}} \approx 1.2 \left(\frac{\rho_{\bullet}}{2 \text{ g cm}^{-3}} \right) \times \left(\frac{\Sigma_g}{300 \text{ g cm}^{-2}} \right)^{-2} \left(\frac{H/r}{0.043} \right) \left(\frac{r}{3 \text{ AU}} \right). \quad (\text{C7})$$

Thus Epstein drag is the relevant regime for the application of our model to particles with $\Omega_K \tau_f \lesssim 1$ beyond $r = 3 \text{ AU}$.

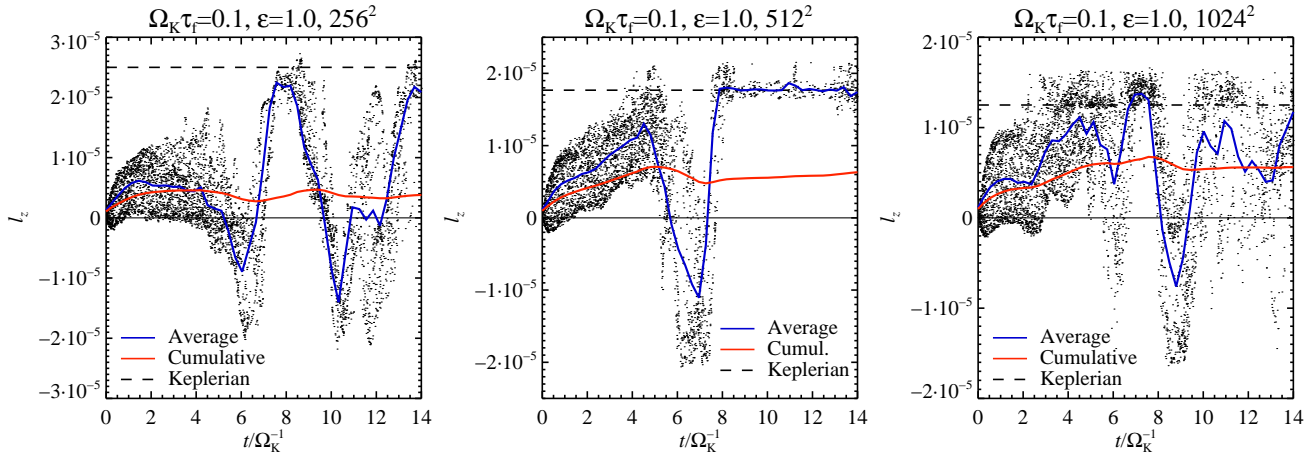


Figure E1. Convergence in grid resolution. The plots show the accreted angular momentum for runs with 256^2 grid points (left panel), 512^2 grid points (middle panel) and 1024^2 grid points (right panel). In all cases a net positive angular momentum is accreted, although periods of retrograde accretion occur as well. The inner radius of the simulations, where particles are considered to be accreted to the protoplanet, is reduced proportional to the resolution.

APPENDIX D: PARTICLE COLLISIONS

In this section we argue that particle collisions are negligible compared to gas drag in most of the simulation domain. The time-scale for collisions between particles is

$$\tau_c = \frac{\lambda_p}{c_p}, \quad (\text{D1})$$

where c_p is the local velocity dispersion (“temperature”) of the particles and λ_p is the mean free path for particle collisions. The mean free path in a granular medium can be calculated from the particle number density n_p and collisional cross section σ_p ,

$$\lambda_p = \frac{1}{n_p \sigma_p}. \quad (\text{D2})$$

Assuming spherical particles of radius a , this yields a collision time-scale

$$\tau_c = \frac{a \rho_\bullet}{3 c_p \rho_p}. \quad (\text{D3})$$

The ratio of Epstein friction time to collision time is (ignoring factors of order unity)

$$\frac{\tau_f}{\tau_c} \approx \frac{c_p \rho_p}{c_s \rho_g}. \quad (\text{D4})$$

Particle collisions become important when $\rho_p/\rho_g \gtrsim c_s/c_p$, i.e. for flows with large particle loading. For the typical value $c_p \approx 0.01 c_s$, particle collisions are important when $\rho_p/\rho_g \gtrsim 100$. Thus we can ignore particle collisions in the average state of the simulations presented in the main paper. Nevertheless particle collisions will become important in the dense regions close to the protoplanet, and indeed particle collisions may be important for efficient accretion of circumplanetary material onto the protoplanet.

APPENDIX E: CONVERGENCE TEST

To quantify the effect of grid resolution and inner accretion radius on the results presented in the main paper, we

have run lower resolution (256^2 grid points, 250,000 particles) and higher resolution (1024^2 grid points, 8,000,000 particles) variations of the main simulation. We set the inner accretion radius to 4 grid points in all cases. The accreted angular momentum is shown in Fig. E1. It is clear that the behaviour at all three resolutions is highly time variable, with periods of prograde and retrograde accretion interspersed. However, in all cases a net positive angular momentum is accreted, inducing between 25% and 50% of the surface Keplerian frequency to the protoplanet. There is a trend for accreting stronger prograde rotation with increasing resolution.

APPENDIX F: DEPENDENCE ON BOX SIZE

We proceed to test the dependence of our results on the size of the simulation domain. For this purpose we ran a low resolution simulation with the radial and azimuthal extent expanded by a factor 2.5, to $L_x = L_y = 0.1$. We kept the grid and particle resolution constant by using 640×640 grid cells and 1,562,500 particles, corresponding in resolution to the 256^2 simulation shown in the left panel of Fig. E1. The accreted angular momentum is shown in Fig. F1. The larger box size has a net positive effect on the prograde rotation of the protoplanet. The sign of the angular momentum is more consistently positive than in the small box, and there are fewer periods of retrograde accretion.

This paper has been typeset from a $\text{T}_\text{E}\text{X}/\text{L}^\text{A}\text{T}_\text{E}\text{X}$ file prepared by the author.

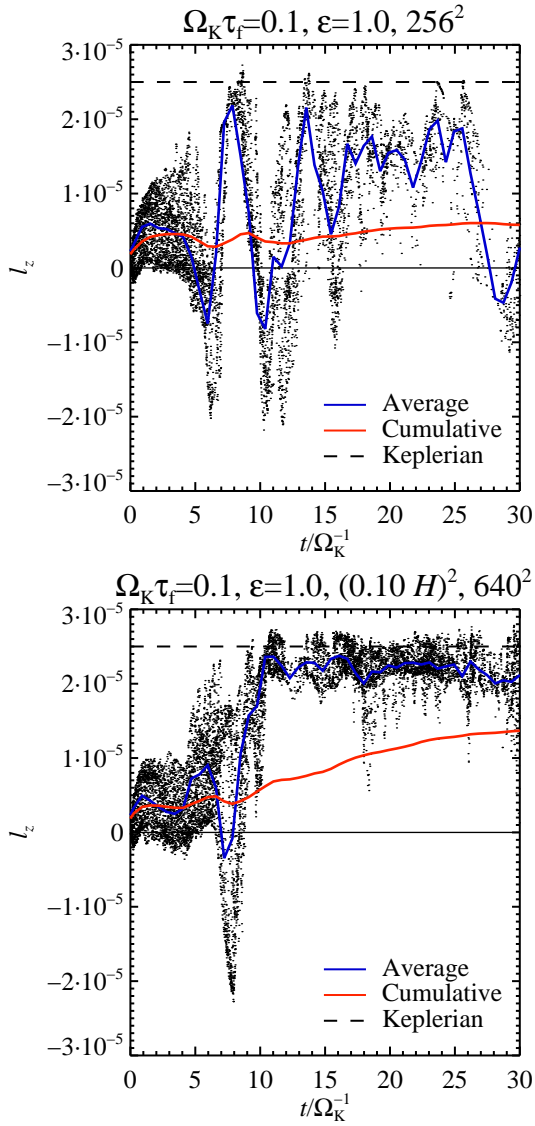


Figure F1. Convergence in box size. The plots show the accreted angular momentum for low resolution runs with $L_x = L_y = 0.04H$ (top panel) and $L_x = L_y = 0.1H$ (bottom panel). Prograde motion is more readily accreted to the protoplanet in the larger box.